

Effects of Surface Treatment on Fretting Fatigue Performance of Ti-6Al-4V

Mr. Michael J. Shepard

Air Force Research Laboratory, Materials and Manufacturing Directorate
Wright-Patterson AFB, OH, 45433-7817

Mr. Paul S. Prevéy and Dr. N. Jayaraman

Director of Research, Lambda Research
Cincinnati, OH 45227-3401

ABSTRACT

The fretting fatigue performance of Ti-6Al-4V after isothermal exposure was explored in test coupons in low plasticity burnished (LPB), shot peened (SP) and electropolished (ELP) baseline conditions. The thermal stability of the compressive residual stress fields produced by SP and LPB was investigated. In the current study, fretting fatigue data and fractography are presented along with in-depth residual stress profiles, both before and after the isothermal exposure. Surface roughness data for each of the three surface conditions are reported.

INTRODUCTION

Often, turbine engine components are retired from service before "full life" is reached. Among the most common reasons is accumulated fretting damage in the dovetail slots of the disks. This fretting damage is very difficult to characterize and analyze. As such, prudence often dictates that the components be removed from service before their full design life. Due to the long lead times and the high costs associated with replacing this hardware, it would be desirable to have a comprehensive set of tools to avoid, minimize sensitivity to, or repair fretting damage. This package of tools will likely include a number of elements including new design approaches to minimize contact stresses, coating systems to minimize fretting damage, and surface treatments to mitigate the effects of any fretting damage.

Shot peening, the most common surface treatment has long been used to increase fretting fatigue performance. [1,2] More recently it has been demonstrated that other surface treatment approaches, such as laser shock processing

(LSP) can have a beneficial effect on fretting fatigue performance. [3] The improvement in fretting fatigue performance is due to the in-depth compressive residual stress field and perhaps, in the case of shot peening, the associated work hardening. The purpose of the current effort is to demonstrate the feasibility of using a third process, low plasticity burnishing (LPB), to improve fretting fatigue performance.

LPB is essentially an advanced CNC controlled burnishing process, a detailed description of the process and other applications of the process can be found elsewhere. [4-7] LPB can be used to induce deep, high magnitude compressive residual stresses in metallic systems and may provide an affordable, high performance process for fretting fatigue enhancement.

It is proposed that the principal mechanism for fretting fatigue improvement due to component surface treatments is the retardation of fatigue crack growth due to the compressive residual stresses. The contact stresses associated with the disk-dovetail configurations can potentially be well above the yield stress of the material. These contact stresses diminish rapidly with increasing depth, however. As such, in the worst-case scenario it is useful to consider the surface material largely "sacrificial." The applied contact stresses can be sufficiently high that the nucleation and growth of fretting fatigue cracks is unavoidable. These small cracks are initially driven by a combination of the contact stresses and the bulk stresses. As the contact stresses diminish with increasing crack length (depth), the driving force for crack growth becomes the bulk stress. In an untreated component, or one where the surface treatment produces only a shallow compressive residual stress, the crack may be

Proceedings of the 8th National Turbine Engine High Cycle Fatigue (HCF) Conference
April 14-16, Monterey, CA, 2003

beyond the fatigue crack growth threshold stress intensity factor range and the crack might continue to grow to failure. In a component with a deeper compressive residual stress field, such as those generated by LPB, the compressive residual stresses may act to arrest or significantly retard the growth of the fatigue crack once it is driven primarily by the bulk stresses.

EXPERIMENTAL

Specimen Preparation

Specimens for the experimental program were excised from two mill-annealed Ti-6Al-4V plates produced as per AMS 4911H. Material chemistry and average mechanical properties for each of the plates are summarized in Table I.

A thick section, 4-point bend fatigue sample with a trapezoidal gage cross section was used for the fretting fatigue testing. The trapezoidal cross section HCF sample was designed specifically for testing component surface treatments. This specimen design is extremely useful since it forces fatigue failures to initiate in the gage section even though the residual stresses due to surface treatment are highly compressive.

For the specimens subjected to LPB and shot peening, the entire gage section was treated. LPB parameters were optimized by Surface Enhancement Technologies, LLC to maximize the magnitude and depth of the compressive residual stresses, while minimizing cold work. Figure 1 depicts the LPB process being applied to a batch of specimens similar to those used in this study. Specimens subjected to shot peening were peened to a 6-8A Almen intensity, 125% coverage, with CCW14 shot. This level of shot peening is representative of that used for Ti-6Al-4V engine hardware.

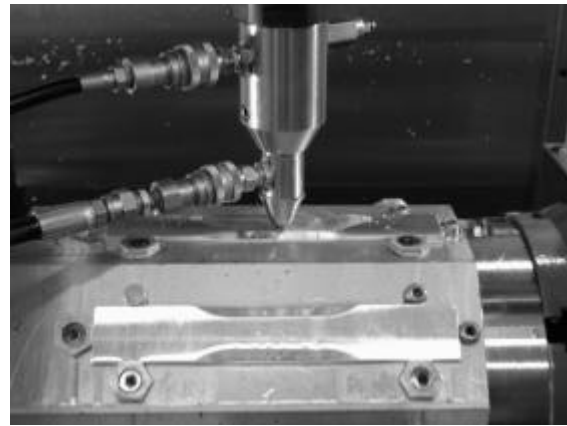


Figure 1. LPB Processing of the thick section fatigue specimen in the four-axis manipulator on the CNC milling machine

For the “stress-free” electropolished baseline, nominally 0.003 in. of material was removed from the surface of the fatigue specimen gage. Xray diffraction residual stress measurements were made on a portion of the samples to verify negligible residual stress and cold working existed after electro polishing.

Specimens were thermally treated to simulate elevated temperature exposure under engine operating conditions. Isothermal exposures were conducted in lab air. Exposures were at 375C for 10 hours, followed by an air cool. This temperature is representative of an aggressive use temperature for Ti-6Al-4V.

X-Ray Diffraction Residual Stress and Cold Work Measurement

X-ray diffraction residual stress measurements were made at the surface and at several depths below the surface on LPB and shot peened fatigue specimens. Measurements were made before and after the 375C/10 hr. thermal exposure to determine the degree of stress relaxation. Reported stresses are for the residual

Table I
Material chemistry and mechanical properties of Ti-6Al-4V alloy used in this study:

Heat Number	Element (Weight Percent)							Mechanical Properties			
	C	N	Fe	O	Al	V	Y	Yield Strength (ksi)	UTS (ksi)	Elong. (%)	Reduct. of Area (%)
D002776	.03	.02	.18	.18	5.96	4.16	<.001	133	141	14	43
528EW	.02	.01	.18	.16	6.14	3.78	<.001	133	139	14	40

stress component oriented parallel to the longitudinal axis of the specimen.

X-ray diffraction residual stress measurements were made employing a $\sin^2\psi$ technique and the diffraction of copper $K\alpha_1$ radiation from the (21.3) planes, of the Ti-6Al-4V. It was first verified that the lattice spacing was a linear function of $\sin^2\psi$ as required for the plane stress linear elastic residual stress model.[8-11]

Material was removed electrolytically for subsurface measurement in order to minimize possible alteration of the subsurface residual stress distribution as a result of material removal. The residual stress measurements were corrected for both the penetration of the radiation into the subsurface stress gradient [12] and for stress relaxation caused by layer removal.[13]

The value of the x-ray elastic constants required to calculate the macroscopic residual stress from the strain normal to the (21.3) planes of the Ti-6Al-4V were determined in accordance with ASTM E1426-91. [14] Systematic errors were monitored per ASTM specification E915.

Measurements of cold work are based on analysis of x-ray diffraction peak broadening. The breadth of the x-ray diffraction peaks is calibrated empirically by using specimens made from identical material that are deformed to known levels of cold work.[15]

High Cycle and Fretting Fatigue Testing

Fretting fatigue testing was conducted under constant amplitude 4-pt. bend loading on a Sonntag SF-1U fatigue machine. The SF-1U is modified for fretting fatigue testing by clamping a bridge-type fretting device to the gage section of the fatigue specimen using an instrumented loading ring clamp, similar to the apparatus described by Frost, Marsh, and Pook [16]. A photo of the fatigue test setup is shown in Figure 2.

The fretting bridge contains two 0.25 in. diameter Ti-6Al-4V cylindrical pins, nominally 0.5 in. apart, yielding a cylinder-on-flat contact geometry. The cylindrical pins were not surface treated. The contact geometry was not selected to be

representative of any particular engine geometry. The intent was to generate a significant debit in fatigue performance due to contact damage. A photograph of the assembled fretting fatigue fixture is shown in Figure 3.

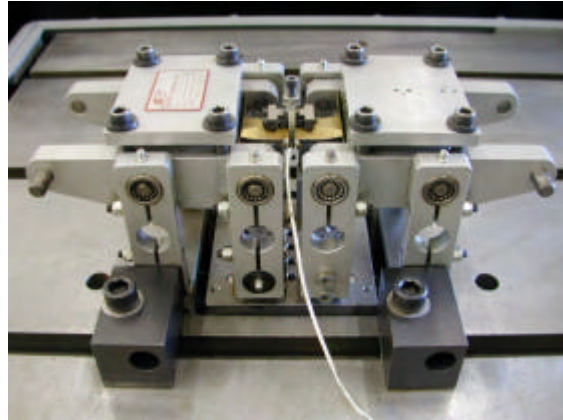


Figure 2. HCF (4-point bending) testing set up with the fretting fixture mounted on the specimen.



Figure 3. Fretting fixture with instrumented loading ring and bridge device to hold two fretting cylindrical pins clamped on to the fatigue specimen surface under a controlled normal force.

All testing was conducted at ambient temperature (~72F) at 30Hz with an applied stress ratio $R = 0.1$. Prior to the start of each test, a 150 lb. normal load was placed on the loading ring for the fretting bridge. Tests were conducted to specimen fracture or a "run-out" life of 2.5×10^6 cycles. Run-out specimens were subsequently fatigue "re-tested" to fracture at 20 ksi or greater maximum applied stress above the run-out stress. Run-out samples were re-loaded without disturbing the

fretting bridge by simply increasing the load and restarting the fatigue test.

Surface Roughness Measurement

The surface roughness values were obtained using a Mitutoyo SJ-201 Surface Roughness Tester. The Ra surface roughness, defined as the arithmetic mean of the absolute values of the profile deviations from the mean line, was calculated over a 0.150 in. evaluation length perpendicular to the specimen axis and over a 0.5 in. evaluation length parallel to the specimen axis. A measurement performed on a 116 μin standard resulted in a value of 116.1 μin.

Fractography

Following fatigue testing, each specimen was examined optically at magnifications up to 60X to identify fatigue origins and locations thereof relative to the specimen geometry. Pictures were taken with a Nikon 990 digital camera through a Nikon Stereoscopic microscope at 15x. A representative photograph of a typical failure for each specimen group was obtained. A few selected specimens were also examined under a Hitachi S500 SEM equipped with EDAX.

RESULTS AND DISCUSSION

Residual Stresses and Thermal Stability

The residual stress distributions measured as functions of depth are shown graphically in Figures 4 through 7. Compressive stresses are shown as negative values, tensile as positive, in units of ksi (10^3 psi) and MPa (10^6 N/m²).

Figures 4-7 show the residual stress (RS) and % cold work (CW) profiles for specimens subjected to low stress grinding (LSG) and buffing, shot peening (SP) and low plasticity burnishing (LPB) treatments. RS and CW profiles of a specimen finished with a buffing wheel are included for the sake of baseline comparison. For SP and LPB conditions, the effect of prolonged exposure to an elevated temperature of 375C for 10hrs to simulate the components' engine operating conditions was also studied.

Figure 4 shows the RS and CW profiles of the specimen surface after a low stress grind (LSG)

and buffing treatment. The surface is in compression at -60 ksi with cold work of about 35%. The compression drops off to near zero within the first 0.001 in., and the %CW drops off to zero within the first 0.0003 in. depth.

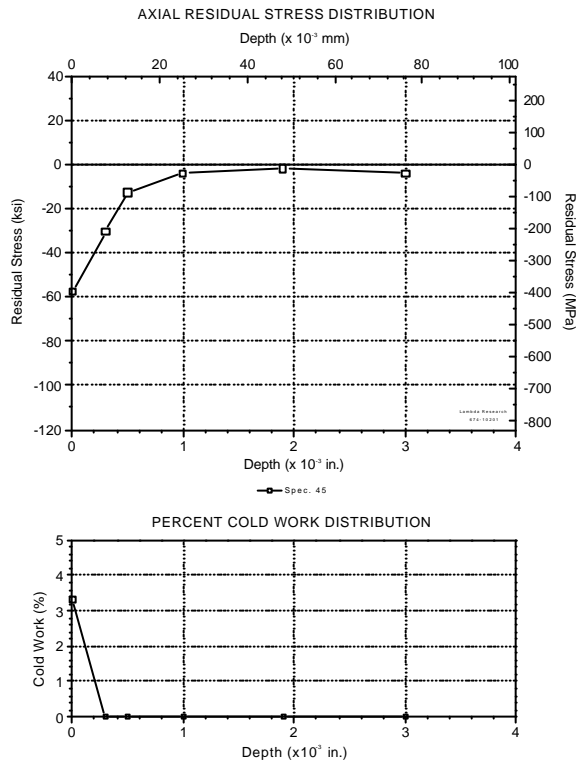


Figure 4 – RS & CW profile for Ti-6-4 finished with low stress grinding (LSG) and buffing showing the resulting depth of compression less than 0.001 in.

Figure 5 shows the RS and CW profiles for a shot peened surface. The SP surface compression is nominally -110 ksi, and drops off to zero somewhat erratically over a depth of about 0.007 in. Upon thermal exposure to 375C for 10 hrs, the surface compression drastically changes to nominally -15 ksi, as has been observed repeatedly for highly cold worked Ti and Ni alloys. Maximum subsurface compression of nominally -80 ksi occurs at a depth of 0.004 in., and drops off to zero at a depth of nominally 0.007 in. Correspondingly, %CW is a little over 65% on the surface, which drops off to zero at a depth of about 0.003 in. The high surface %CW decreases to 35% upon thermal exposure.

The RS and CW profiles for LPB treated surface are shown in Figure 6. Surface compression is nominally -35 ksi. Maximum compression of -105 ksi occurs at a depth of .005 to .010 in., and

drops off to zero at a depth of over 0.040 in. Upon thermal exposure to 375C for 10 hrs, the surface RS changes to about -20 ksi, but the subsurface maximum remains at -150 ksi, and the depth is unaffected. Correspondingly, %CW is a little under 30% on the surface, and drops off to less than 5% at a depth of about .002 in., and then gradually to zero at 0.015 in. The initial level of surface cold work is attributed to prior LSG preparation of the surface. The surface %CW decreases to 15% upon thermal exposure.

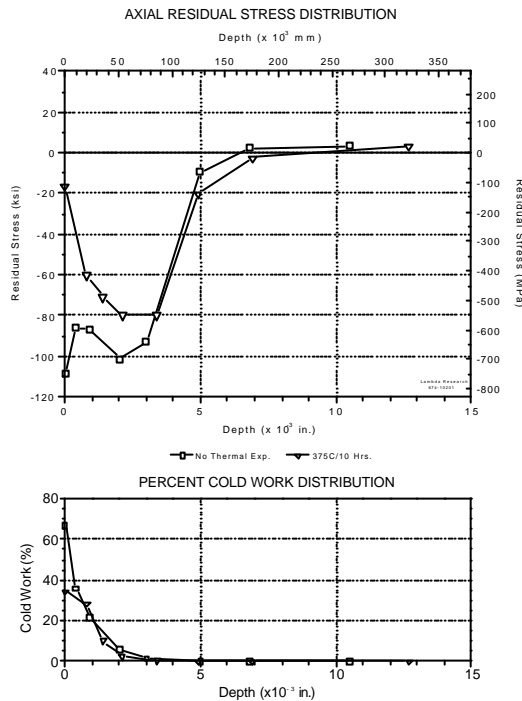


Figure 5 – RS & CW profile for SP showing a depth of compression up to about 0.007 in. and loss of surface compression after thermal exposure

Surface Roughness

Surface roughness of LPB, electropolished, and Shot Peened surfaces are shown in Figure 7. A representative bar chart of the average surface roughness for LPB, baseline (electropolished - ELP), and shot peened surfaces are shown in Figure 7. The baseline electropolished samples had surface roughness values in the 15 to 20 μin range. The surface roughness was less than 5 μin for the LPB processed samples. This is considerably lower roughness than the surface produced by the shot peening operation. With surface roughness ranging from 80 to 100 μin., this surface was the roughest in the study.

Effect of Surface Treatments on HCF Performance and FOD Tolerance of a Ti-6Al-4V Vane

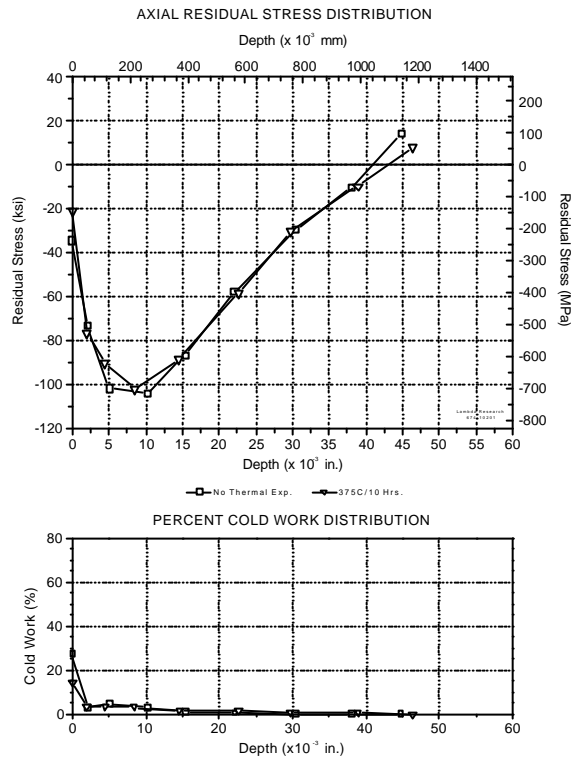


Figure 6 – RS & CW profile for LPB. Note the depth of compression is over 0.04 in. and is not significantly altered by thermal exposure to 375C for 10 hr.

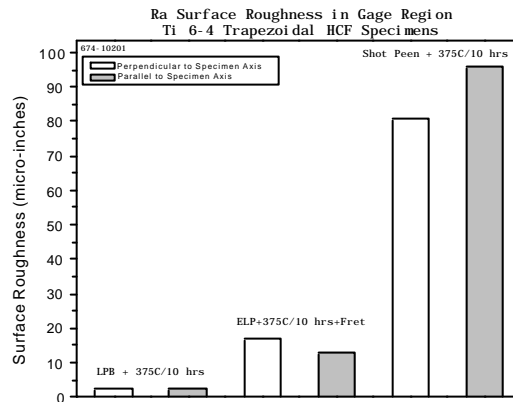


Figure 7. Comparison of surface roughness for ELP, SP and LPB treated specimens.

Fatigue and Fretting Fatigue

The HCF fretting fatigue tests are presented graphically as S-N curves in Figures 8 through 10. The data are shown in a semi-log plot of maximum stress in units of ksi (10³ psi) and MPa vs. cycles to failure. Figure 8 contains the high cycle fatigue data (no-fretting) for the LPB'd, shot

peened and electropolished specimens. The beneficial effects of both SP and LPB treatments are apparent. LPB clearly outperforms SP in the high stress, the finite life regime, where crack propagation dominates total life. In the lower stress, longer life regime, where life is dominated by crack initiation, both SP and LPB showed similar HCF performance. For the ELP'd and SP'd specimens all observed failures originated from surface initiated cracks.

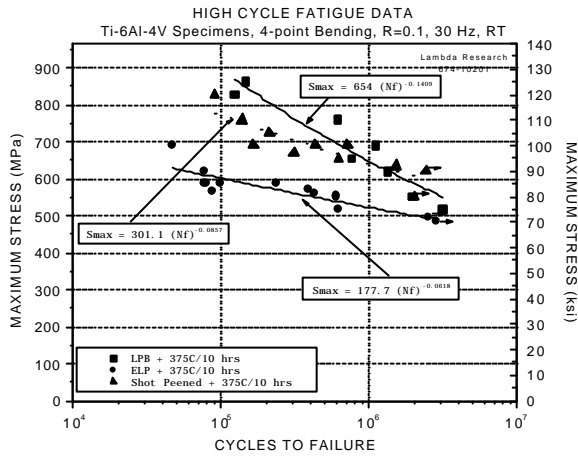


Figure 8. Baseline HCF data for ELP, SP and LPB treated specimens – Note that the HCF performance of LPB is superior despite the fact that sub surface crack initiation was dominant.

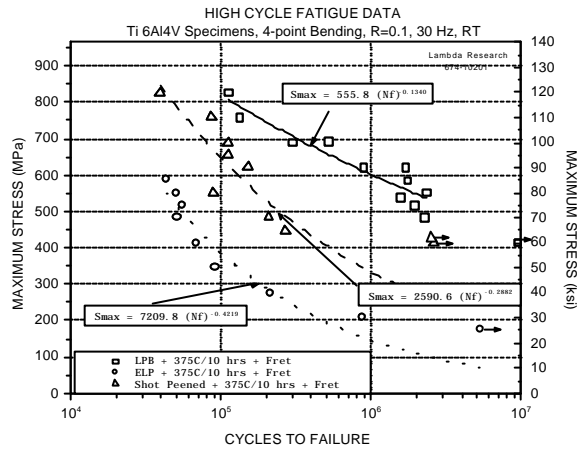


Figure 9. Comparison of fretting HCF data for ELP, SP and LPB treated specimens.

In the LPB treated specimens sub-surface initiation sites were the mode of failure. Initiation was invariably below the compressive residual

stress layer near the sharp corners of the thick section fatigue specimens. Two reasons exist for this failure mode. First, the specimen surface, which is the usual fatigue crack initiation site, is considerably improved in terms of both surface finish and residual stress state. Secondly, subsurface residual stresses must eventually transition to compensatory tension to equilibrate the nearer surface compressive residual stresses generated by the LPB process. These compensatory tensile stresses, in conjunction with the applied stresses now act as the predominant failure driver. It should be emphasized, however, that even though subsurface initiation was predominant in the LPB'd specimens, their performance was at least equal to that of shot peened specimens, and in the finite life regime, was considerably better.

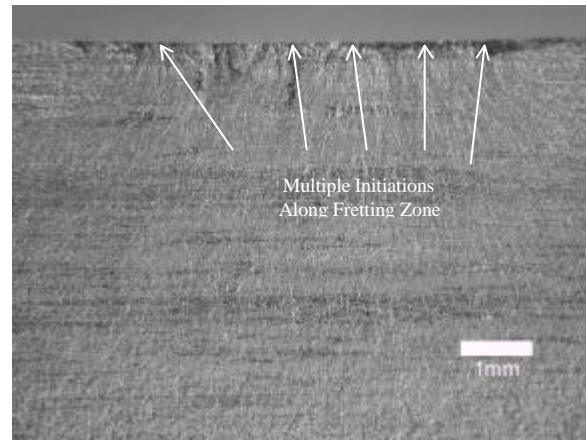


Figure 10. Low magnification optical fractograph of ELP treated specimen. Failure occurred from initiated cracks under the fretting scars. Note the dark band near the surface indicative of the fretting damage zone leading to multiple crack initiation sites. (ELP+Thermal+Fret Specimen 82, Smax=50 ksi, and Nf=91,814)

Figure 9 contains the fretting fatigue data for the LPB'd, SP'd and electropolished (ELP) specimens. The benefits of surface treatment, particularly LPB, for this fretting configuration are clear. In the baseline condition, fretting damage has dropped the 2.5×10^6 cycle fatigue strength from nominally 70 ksi max stress to nominally 25 ksi max stress, and the fatigue life at all stress levels is drastically reduced. A typical fracture surface for the ELP condition, with multiple initiation sites at the fretting damage is shown in Figure 10. In the case of the SP treated

specimens, the 2.5×10^6 cycle fatigue strength decreased from nominally 85 ksi to 60 ksi, and similar to the baseline condition, at all stress levels the fatigue lives were considerably lower. A typical fracture surface for the SP'd condition is shown in Figure 11. Similar to the ELP'd condition, multiple initiation sites are observed at the fretting damage. All initiation sites for the baseline and SP'd condition were observed to be associated with fretting damage.

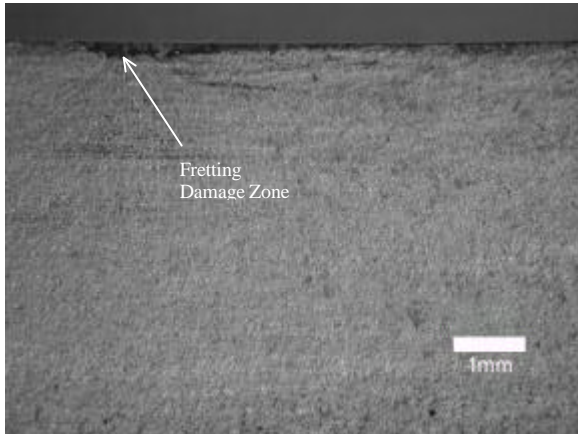


Figure 11. Low magnification optical fractograph of SP treated specimen. Failure occurred from initiated cracks under the fretting scars. Note the dark band near the surface indicative of the fretting damage zone leading to a crack initiation site. (SP+Thermal+Fret Specimen 76, $S_{max}=95$ ksi, and $N_f=111,093$)

The performance of the LPB'd specimens subjected to fretting damage was largely identical to the performance without fretting damage. This is further born out by the fact that, as with the high cycle fatigue testing discussed earlier, all of the failure initiation sites in the LPB processed specimens were subsurface. Failures did not originate from the fretting damaged regions in the LPB'd specimens. This mitigation of the fretting fatigue damage by LPB is depicted more clearly in Figure 12. A typical fracture surface for the LPB'd + fretting condition is shown in Figure 13. Note that the initiation site is subsurface and occurred on a plane remote from the fretting fatigue damage.

This fracture behavior suggests that the deep, high magnitude compressive residual stresses induced by LPB, have prevented any critical crack growth from the fretting scars. Rather, the LPB

induced residual stresses have largely eliminated the debit in high cycle fatigue performance from fretting damage.

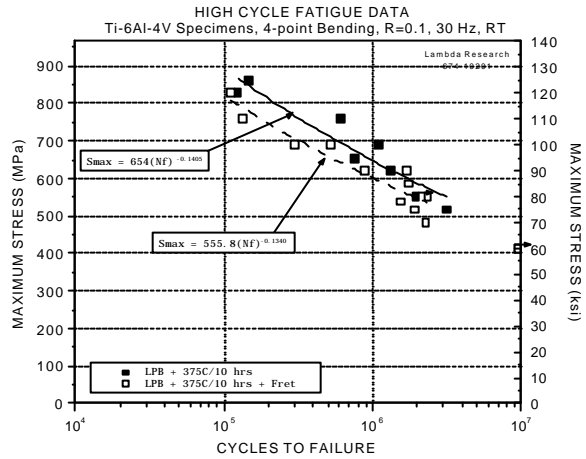


Figure 12. HCF data for LPB treated specimen with and without fretting. The effect of fretting on both HCF performance and the endurance limit is minimal

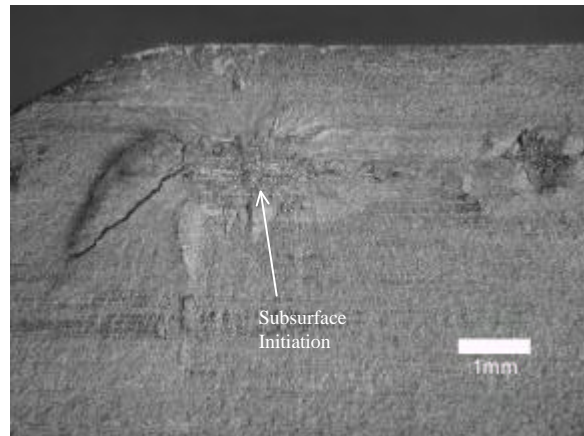


Figure 13. Low magnification optical fractograph of LPB treated specimen. Failure initiated subsurface, on a plane away from the fretting pads, with no regard for the fretting scars. (LPB+Thermal Specimen 6, $S_{max}=85$ ksi, and $N_f=1,303,823$)

CONCLUSIONS

The subject study has demonstrated the benefits of shot peening and particularly low plasticity burnishing on Ti-6Al-4V specimens in a fretting fatigue environment. While both surface treatments provided a clear benefit over the baseline condition, the performance of LPB treated specimens was superior. This is attributed

to the enhanced surface finish and the deeper, more thermally stable compressive residual stresses associated with the LPB treated specimens.

REFERENCES

1. Waterhouse, R.B. and Saunders, D. A., "The Effect of Shot Peening on the Fretting Fatigue Behavior of an Austenitic Stainless Steel and a Mild Steel," *WEAR Magazine*, No. 53 (1979), pp. 381-386.
2. Waters, K. T., "Production Methods of Cold Working Joints Subjected to Fretting for Improvement of Fatigue Strength," Presented at the Third Pacific Area National Meeting of ASTM, San Francisco, CA, October 11-16, 1959.
3. T. N. Farris, H. Murthy, E. Pérez-Ruberté, P. T. Rajeev, "Experimental Characterization of Fretting Fatigue of Engine Alloys," *Proceedings: 6th Nat. Turbine Eng. HCF Conference*, 2001
4. P.S. Prevéy, J. Telesman, T. Gabb and P. Kantzos, "FOD Resistance and Fatigue Crack Arrest in Low Plasticity Burnished IN718," *Proceedings of the 5th Nat. Turbine Eng. HCF Conference*, 2000.
5. J.T. Cammett, P.S. Prevéy, "Low Cost Corrosion Damage Mitigation and Improved Fatigue Performance of Low Plasticity Burnished 7075-T6," *Proceedings of the 4th International Corrosion Workshop*, Aug. 22-25, 2000.
6. P.S. Prevéy, M. Shepard and P. Smith, "The Effect of Low Plasticity Burnishing (LPB) on the HCF Performance and FOD Resistance of Ti-6Al-4V," *Proceedings: 6th Nat. Turbine Eng. HCF Conference*, 2001
7. J. Cammett and P.S. Prevéy, "Fatigue Strength Restoration in Corrosion Pitted 4340 Alloy Steel via Low Plasticity Burnishing," available at <http://www.lambda-research.com/publica.htm>
8. Hilley, M.E. ed.,(1971), Residual Stress Measurement by X-Ray Diffraction, *SAE J784a*, (Warrendale, PA: Society of Auto. Eng.).
9. Noyan, I.C. and Cohen, J.B., (1987) Residual Stress Measurement by Diffraction and Interpretation, (New York, NY: Springer-Verlag).
10. Cullity, B.D., (1978) Elements of X-ray Diffraction, 2nd ed., (Reading, MA: Addison-Wesley), pp. 447-476.
11. Prevéy, P.S., (1986), "X-Ray Diffraction Residual Stress Techniques," *Metals Handbook*, **10**, (Metals Park, OH: ASM), pp 380-392.
12. Koistinen, D.P. and Marburger, R.E., (1964), Transactions of the ASM, **67**.
13. Moore, M.G. and Evans, W.P., (1958) "Mathematical Correction for Stress in Removed Layers in X-Ray Diffraction Residual Stress Analysis," *SAE Transactions*, **66**, pp. 340-345
14. Prevéy, P.S., (1977), "A Method of Determining Elastic Properties of Alloys in Selected Crystallographic Directions for X-Ray Diffraction Residual Stress Measurement," Adv. In X-Ray Analysis, **20**, (New York, NY: Plenum Press, 1977), pp 345-354.
15. Prevéy, P.S., "The Measurement of Subsurface Residual Stress and Cold Work Distributions in Nickel Base Alloys", Residual Stress in Design, Process and Materials Selection, W.B.Young, ed., ASM, Metals Park , OH, 1987, pp 11-19.
16. N.E. Frost, K.J. Marsh and L.P. Pook, Metal Fatigue, Oxford University Press, Oxford, UK, 1974, pp 364-370, Fig. 6.23.